Controls of Quasi-Linear Convective System Tornado Intensity

GEOFFREY R. MARION[a] AND ROBERT J. TRAPP[a]

[a] *University of Illinois at Urbana–Champaign, Urbana, Illinois*

ABSTRACT: Although tornadoes produced by quasi-linear convective systems (QLCSs) generally are weak and short lived, they have high societal impact due to their proclivity to develop over short time scales, within the cool season, and during nighttime hours. Precisely why they are weak and short lived is not well understood, although recent work suggests that QLCS updraft width may act as a limitation to tornado intensity. Herein, idealized simulations of tornadic QLCSs are performed with variations in hodograph shape and length as well as initiation mechanism to determine the controls of tornado intensity. Generally, the addition of hodograph curvature in these experiments results in stronger, longer-lived tornadic-like vortices (TLVs). A strong correlation between low-level mesocyclone width and TLV intensity is identified ($R^2 = 0.61$), with a weaker correlation in the low-level updraft intensity ($R^2 = 0.41$). The tilt and depth of the updraft are found to have little correlation to tornado intensity. Comparing QLCS and isolated supercell updrafts within these simulations, the QLCS updrafts are less persistent, with the standard deviations of low-level vertical velocity and updraft helicity approximately 48% and 117% greater, respectively. A forcing decomposition reveals that the QLCS cold pool plays a direct role in the development of the low-level updraft, providing the benefit of additional forcing for ascent while also having potentially deleterious effects on both the low-level updraft and near-surface rotation. The negative impact of the cold pool ultimately serves to limit the persistence of rotating updraft cores within the QLCS.

KEYWORDS: Convective storms/systems; Severe storms; Convective storms; Convection lines; Convective-scale processes; Tornadoes

1. Introduction

Historically, tornado research largely has focused on supercell thunderstorms, which are responsible for a significant portion of total tornadoes as well as most strong tornadoes (Trapp et al. 2005; Smith et al. 2012). Quasi-linear convective systems (QLCSs), by comparison, have received little attention in the literature, despite contributing over 21% of tornadoes in the United States each year (Trapp et al. 2005; Smith et al. 2012; Ashley et al. 2019). In other countries such as the United Kingdom (e.g., Mulder and Schultz 2015) and Japan (e.g., Kobayashi et al. 2007; Sugawara and Kobayashi 2009), QLCSs as well as narrow cold-frontal rainbands contribute an even higher percentage of annual tornadoes.

QLCS tornadoes are more likely than supercell tornadoes to occur overnight (Trapp et al. 2005) and during cool-season months (October–February; Trapp et al. 2005; Smith et al. 2012). Because of these characteristics as well as their inherently short warning lead times (Trapp et al. 1999; Brotzge et al. 2013), QLCSs tornadoes are particularly dangerous to vulnerable populations (Ashley 2007; Ashley et al. 2008). However, QLCS tornadoes also tend to be weaker than their supercell counterparts, with enhanced Fujita (EF) ratings of QLCS tornadoes rarely exceeding EF-2 (Trapp et al. 2005; Smith et al. 2012). Such limits on QLCS tornado intensity are of fundamental interest herein.

QLCS tornadoes are known to form within mesovortices, particularly the deepest and strongest within a given QLCS (Atkins et al. 2004); nontornadic mesovortices, however, can still be hazardous, because they are capable of causing severe

"straight-line" winds (e.g., Funk et al. 1999; Przybylinski et al. 2000; Trapp and Weisman 2003; Atkins et al. 2005; Wheatley et al. 2006). Przybylinski (1995) speculated that mesovortices and QLCS tornadoes are most apt to result from interactions between a QLCS and environmental heterogeneities such as outflow boundaries, although the nature of these interactions is perhaps not as originally envisioned. Specifically, Wheatley and Trapp (2008) found in simulations that the primary contribution of an external boundary to QLCS mesovortex genesis was an enhancement of horizontal convergence, rather than the tilting of horizontal baroclinic vorticity associated with the boundary.

Internal QLCS processes have also been linked to QLCS mesovortex formation, including the release of horizontal shear instability (HSI; Haurwitz 1949; Miles and Howard 1964), as demonstrated through an observational analysis by Carbone (1982, 1983) and then through idealized modeling by Lee and Wilhelmson (1997a,b). Subsequent studies by Wheatley and Trapp (2008), Smart and Browning (2009), and Conrad and Knupp (2019) have confirmed the role of HSI in QLCS mesovortex/tornado formation.

Another internal process resulting in mesovortex formation is the upward or downward tilting of environmental or baroclinically generated horizontal vorticity (e.g., Weisman and Trapp 2003; Wheatley and Trapp 2008; Atkins and St. Laurent 2009b; Richter et al. 2014). Low-level vertical vorticity generated through such tilting processes may also combine with vertical vorticity generated along gust fronts through the tilting of environmental horizontal vorticity to aid in mesovortex genesis (e.g., Przybylinski et al. 2000; Atkins and St. Laurent 2009b; Flournoy and Coniglio 2019).

Mesovortex genesis through these tilting processes has been shown to depend on the existence of sufficient environmental vertical wind shear, which supports the development of upright

updrafts (e.g., Weisman and Trapp 2003; Atkins and St. Laurent 2009a; Schaumann and Przybylinski 2012) via a balance between the QLCS cold pool and environmental vertical wind shear (Rotunno et al. 1988). It has not yet been demonstrated, however, whether upright updrafts relate to QLCS tornado intensity, nor has it been demonstrated whether—and how—vertical wind shear influences QLCS tornado intensity, though recent work has examined the relationship between vertical wind shear and the characteristics of mesovortices within a QLCS (Flournoy and Coniglio 2019). Indeed, a question remains as to why QLCS tornadoes reach strong-to-violent intensity more infrequently than supercell tornadoes, despite occurring in environments with a similar range of vertical wind shear and, in some cases, similar thermodynamic characteristics (Smith et al. 2012).

Though the details of the internal processes associated with QLCS tornadogenesis and tornado intensification likely differ from those of supercell tornadogenesis and intensification, the similar environments supportive of strong QLCS and supercell tornadoes (Thompson et al. 2012) suggest some commonalities in basic processes and, consequently, suggests possible applicability of numerous studies of supercell tornadogenesis to the topic of QLCS tornado intensity explored herein. For example, as found previously, low-level vertical wind shear appears to significantly impact the development of a low-level mesocyclone, generating stronger vertical accelerations due to the strong low-level rotation (e.g., Markowski and Richardson 2014). Additionally, it has been hypothesized that the nature of low-level horizontal vorticity (i.e., streamwise versus crosswise) may impact the steadiness of low-level mesocyclones, which may impact tornado formation (e.g., Coffer and Parker 2017).

Similarly, the near-surface (0–500 m) storm-relative helicity (SRH) may serve as a discriminator between tornadic and nontornadic supercell environments, with larger near-surface SRH generally associated with stronger tornadoes (e.g., Coffer and Parker 2017; Flournoy et al. 2020), potentially through its impact on the intensity of the low-level mesocyclone. The connection between low-level mesocyclone intensity and tornado intensity may not be as straightforward as it seems, however. Previous work has noted that, for the extensively studied Goshen County, Wyoming, tornado of 5 June 2009, low-level mesocyclone intensity was not well correlated to the intensity of the tornado (e.g., Atkins et al. 2012). Indeed, additional radar observational evidence suggests that mesocyclone intensity may not serve as the primary control of tornado intensity (Sessa and Trapp 2020).

In the case of supercells, environmental shear influences tornado intensity in part through its influence on updraft width. As explained by Marion and Trapp (2019), stronger environmental shear leads to a larger area of dynamical forcing of vertical accelerations and, consequently, a larger updraft. In turn, a larger updraft allows for the formation of a larger mesocyclonic vortex (r_M), as confirmed theoretically and through numerical simulations by Trapp et al. (2017). Finally, a larger mesocyclone implies larger circulation,

$$\sim r_M V_M,$$

where r_M and V_M are the radius and tangential wind speed of the mesocyclone, respectively. By Kelvin's circulation theorem [see Trapp et al. (2017) for limitations], the mesocyclonic circulation should constrain the tornadic circulation, i.e.,

$$r_M V_M \sim r_T V_T,$$

where r_T and V_T are the radius and tangential wind speed of the tornado, respectively. In supercell simulations by Trapp et al. (2017, 2018), tornado-like vortex (TLV) intensity ($\sim V_T$) is shown to depend primarily on mesocyclone area (r_M) and corresponding updraft area. Consistently, analyses of satellite-derived "overshooting tops" (OTs) above tornadic storms exhibit a primary dependence of tornado EF scale ($\sim V_T$) on OT area ($\sim r_M$) (Marion et al. 2019). Similarly, analyses of Doppler radar data exhibit a primary dependence of tornado EF scale ($\sim V_T$) on pretornadic mesocyclone width ($\sim r_M$) (Sessa and Trapp 2020). It is noteworthy that in the radar data analyses, this dependence is weaker for QLCS tornadoes than for supercell tornadoes, implying that the control on QLCS tornado intensity exerted by rotating updraft, or mesocyclone, width is modulated by some internal factor.

We hypothesize that such a modulation is due, in part, to the processes that dominate updraft forcing within QLCSs, namely, cold pool rather than rotational dynamics, which result in less persistent updrafts. Such forcing by cold pools implies that potentially strong outflow within the QLCS may tend to disrupt tornado intensification, and even tornadogenesis, thus contributing to overall weaker tornadoes. Herein, we use idealized simulations to evaluate if rotating updraft width, as modulated by cold-pool depth and strength, discriminates tornado intensity in QLCSs. As with Trapp et al. (2017), this work does not focus *primarily* on how and why QLCS tornadoes form, but rather, presuming a tornado does form, on what controls its potential intensity; we do, however, acknowledge that overlap between these subjects exists, such that factors that increase the likelihood of tornado formation have some impact on the intensity of the tornado that forms.

To this end, in section 2, we describe the method for simulating tornadic QLCSs using an idealized model. Section 3 focuses on analysis of the simulations and exploring the potential influences on tornado intensity in QLCSs, including updraft width. In section 4, we summarize these findings, their implications, and how they may relate to previous findings.

2. Methodology

QLCS simulations are performed using Cloud Model 1 (release 19; Bryan and Fritsch 2002), a cloud-resolving numerical model. The model integration time is 5 h to allow for TLV analysis within mature QLCSs. The model domain is $512 \times 512 \times 18$ km^3. The lowest model grid level is located at 67.5 m, and the vertical grid is defined such that the grid spacing is constant at 125 m over model heights below 3 km, linearly increases to 250 m for model heights between 3 and 9 km, and held constant at 250 m above 9 km. The horizontal grid spacing is 250 m, which is insufficient to fully resolve tornadoes. A horizontal grid spacing of 250 m is, however, sufficient to allow generation of discrete updraft cores, as
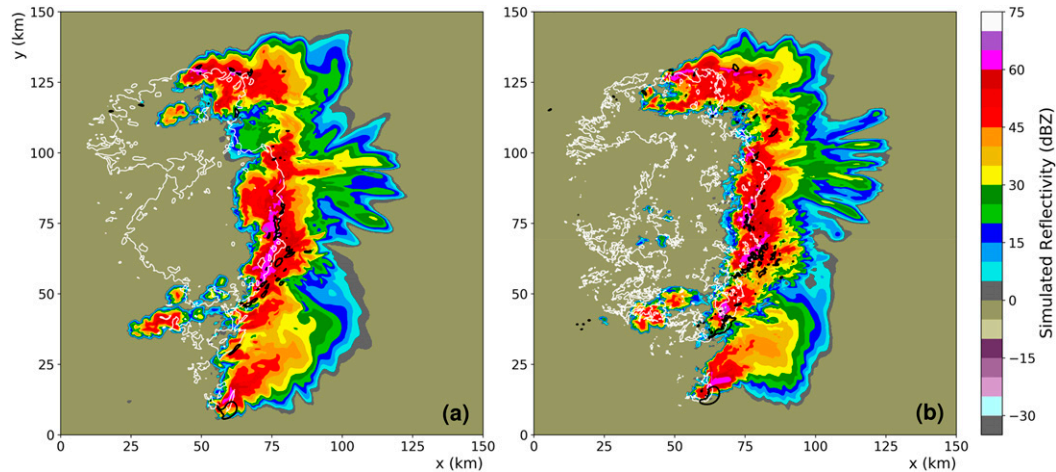
FIG. 1. Horizontal cross section of 1.25 km simulated reflectivity (dBZ; filled contours), vertical velocity ($10 \, m \, s^{-1}$; black contours), and near-surface perturbation potential temperature ($-2 \, K$; white contours) for (a) 250 m and (b) 125 m grid spacing simulations at $t = 130$ min.

shown by Lebo and Morrison (2015). Indeed, comparing test simulations using 250 and 125 m horizontal grid spacing, we find that the general structure of the QLCS remains consistent, with individual updraft cores located within the broad area of ascent near the leading edge of the gust front (Fig. 1). We are primarily interested in these strongest portions of the updraft, such as those associated with strong rotation, as they serve as focal points for TLV formation.

The lateral boundary conditions are open-radiative, and the upper boundary conditions are rigid and free-slip. The lower boundary is also rigid and free-slip: although Schenkman et al. (2012) and others have suggested that surface friction is a key contributor to the TLV development within a numerically simulated QLCS, other studies have shown that TLVs (e.g., Trapp et al. 2018) and even intense, well-resolved tornadoes (Orf et al. 2017) can form in the absence of surface friction. We acknowledge that surface friction is, however, necessary for the existence of endwall vortex structure and associated tornado dynamics, which promotes maximum theoretical vortex intensity (Fiedler and Rotunno 1986; see also Trapp 2000). Nevertheless, the uncertainty surrounding how best to implement friction realistically within models (e.g., Markowski and Bryan 2016; Markowski 2018) ultimately led to its exclusion in these simulations. Additional details on the model configuration are given in Table 1.

Eight simulations are performed, although one simulation did not produce a QLCS, and thus is not analyzed herein. In each of the simulations, the thermodynamic environment is specified as in Marion et al. (2019), and is characteristic of a warm-season severe-convective weather event, with mixed-layer convective available potential energy (MLCAPE) of 2200 J kg^{-1} and lifting condensation level (LCL) of 875 m. This MLCAPE value is equivalent to the upper-quartile climatological value of mixed-layer CAPE for EF1 + QLCS tornadoes during summer (Thompson et al. 2012). We acknowledge that QLCS tornadoes often occur during the cool season in "high shear, low CAPE" (HSLC) environments. However, severe

weather events in these environments appear to have strong links to the details of the synoptic-scale forcing (e.g., Evans and Doswell 2001), which are challenging to fully represent in an idealized model. On the other hand, the less-forced events that occur during the warm season are more amenable to idealized modeling, and thus are pursued here. The high CAPE in typical warm-season QLCS environments also serves to maximize the number TLVs produced. Each of the simulations has an environmental wind profile characterized by a straight or quarter-circle hodograph (Fig. 2). While past modeling studies have used straight hodographs to represent QLCS environments (e.g., Weisman and Trapp 2003; Trapp and Weisman 2003), the climatological study of Smith et al. (2012) suggests that QLCS tornado environments, particularly strong tornado environments, are characterized by significant hodograph curvature. How and why highly curved hodographs appear to result in more intense QLCS tornadoes, however, is not well understood. As such, we seek to understand how QLCS structure and TLV intensity differs for these shear profiles.

For the straight hodographs, the winds increase linearly over the lowest 3 km, and then are held constant above the 3 km level. The quarter-circle hodographs have constant-magnitude winds that trace out a quarter circle over the lowest 1 km.

TABLE 1. Cloud Model 1 (CM1) settings used for simulations.

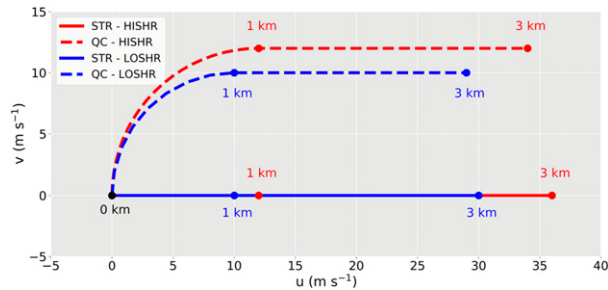|	
Domain	$512 \times 512 \times 18 \, km^3$
Horizontal grid spacing	250 m
Vertical grid spacing	Stretched: 125 m in lowest 3 km, linearly increasing to 250 m at 9 km; constant above
Upper, lower boundary conditions	Rigid, free-slip
Lateral boundary conditions	Open, wave radiating
Microphysical parameterization	NSSL double-moment (Mansell et al. 2010)
Turbulence	TKE (Deardorff 1980)

FIG. 2. Environmental wind hodographs used in QLCS simulations.

Above 1 km, the winds increase linearly to 3 km, and then are held constant above the 3-km level. For each hodograph shape, two 0–3 km bulk wind differences (BWD) are used (30 and 36 m s^{-1}), with the same value over the 0–3 km layer between shapes. The addition of hodograph curvature does result in an increase in the 0–1 km BWD, however, with ranges of 14–18 and 10–12 m s^{-1} for the quarter circle and straight hodographs, respectively. Note that, while the 0–3 km BWD values are on the high end of the QLCS tornado climatological range, the 0–1 km BWD is within the 25th–75th-percentile range of QLCS tornado environments (Thompson et al. 2012).

Convection is initiated via two methods to account for possible differences in TLV intensity that may arise due to differences in QLCS formation. The first method involves a line of five warm bubbles (Fig. 3a), each with a center located at a height of 1.4 km, a vertical radius of 1.4 km, horizontal radius of 10 km, and maximum potential temperature perturbation (θ') of 1.5 K, decreasing radially as $\cos^2 r$, where r is the radius of the bubble. This method of initiation is intended to represent QLCS formation from relatively rapid upscale growth (hereafter UG) of individual cells. Convection is also initiated

using a "cold blob" with center located at the surface (Fig. 3b) with minimum θ' of -12.0 K, decreasing in the x and z directions as $\cos^2 r$, where r is the radius of the cold blob. The cold-blob θ' is constant in the y direction, extending 40 km north and south from the center before also decreasing with $\cos^2 r$. This method represents linearly forced (hereafter LF) convection, and thus QLCS formation via a front or some other boundary where convection is able to move off the initiating boundary (as opposed to, for example, a QLCS that might experience continuous near-field forcing by a strong cold front).

TLVs are identified at the lowest model level (67.5 m) as horizontally contiguous areas exceeding an Okubo–Weiss parameter (hereafter OW; e.g., Markowski et al. 2011) threshold of 10^{-2} s^{-2}; we additionally require that a 10 m s^{-1} updraft at 2 km be located above the near-surface vortex in order to eliminate shallow, nontornadic misovortices from the analysis. We acknowledge that the horizontal grid spacing (250 m) and vertical grid spacing (100 m) are generally too coarse to fully resolve TLVs (e.g., Wicker and Wilhelmson 1995); however, these vortices meet or exceed many criteria generally used to define TLVs. As such, the identification of these vortices as TLVs appears appropriate.

Rotating updrafts (mesocyclones) are identified as horizontally contiguous areas exceeding an OW threshold of 10^{-4} s^{-2} and vertical velocity (w) threshold of 10 m s^{-1} at an altitude of 1.5 km. Note that OW is used to identify these rotating updrafts to limit the effects of deformation on updraft area quantifications, the contributions from which may be substantial in the low levels of the QLCS.

A summary of the TLVs analyzed is given in Table 2. Thirty-four total TLVs are identified, with multiple TLVs from each simulation. Their characteristics and those of their associated updraft are analyzed from 15 min prior to the formation of the TLVs through their dissipation. Within the analysis, we focus
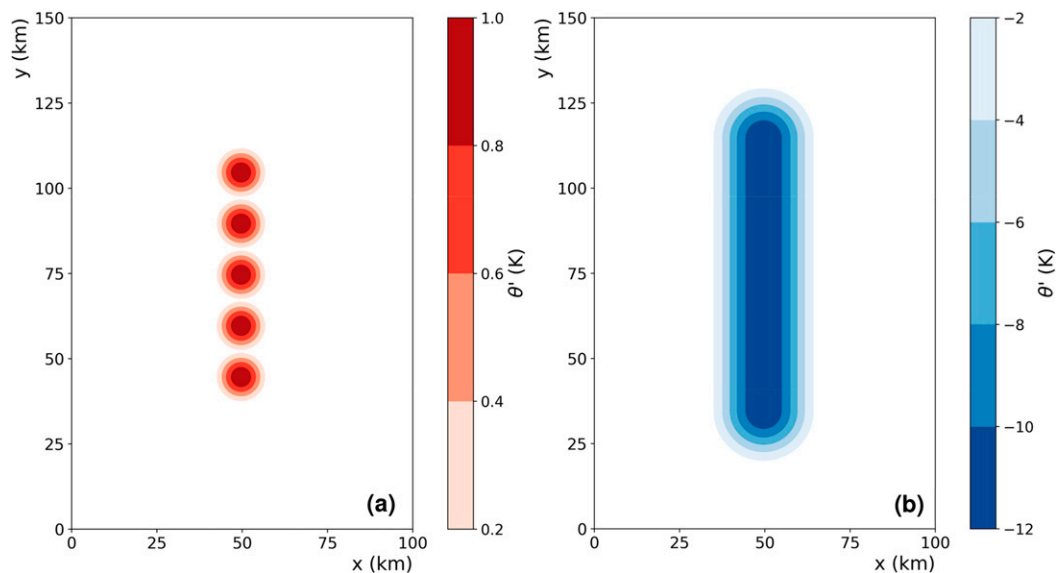

FIG. 3. Horizontal cross section of perturbation potential temperature (θ'; K) for (a) warm bubble initiation (~1.5 km) and (b) cold pool (67.5 m) initiation simulations.

on two time periods, prior to tornadogenesis (pretornadic) and prior to peak tornado intensity, to determine how various storm characteristics during these time periods may correlate to the peak intensity of each tornado. For the purposes of this study, only TLVs within mature QLCSs are analyzed and quantified. Such mature QLCSs meet the criteria of contiguous radar reflectivity exceeding 35 dBZ along a 100-km-long axis (e.g., Trapp et al. 2005).

3. Results

Figure 4 depicts representative "high-end" ($\zeta_{max} = 0.3\,\mathrm{s}^{-1}$) and "low-end" ($\zeta_{max} = 0.133\,\mathrm{s}^{-1}$) QLCS TLVs (see Table 2) at the respective times of their peak intensities. The high-end TLV is associated with a broad, organized (less "slab-like") low-level updraft. The near-surface wind field is strongly convergent beneath the updraft, partly comprised of inflow air with a large fetch within the undisturbed, prestorm environment. Contrastingly, the low-end TLV updraft is more linear, with a much narrower area of ascent at the leading edge of the QLCS. In the near-surface wind field, the flow is relatively weakly convergent ahead of the QLCS, particularly beneath the rotating updraft core associated with the TLV.

In both cases, an area of strong outflow can be found to the south of the TLV (Fig. 4). As will be discussed later, the outflow of the QLCS, which can promote a decoupling between TLV and rotating updraft aloft, has significant implications for TLV persistency and, thus, TLV intensity.

The high-end TLV highlighted in Fig. 4 has a larger horizontal area at its peak intensity than the low-end TLV. Although not all high-end TLVs necessarily have larger areas than low-end TLVs (Fig. 5), we find a positive correlation between their peak TLV area at the lowest model grid level and peak TLV intensity ($R^2 = 0.54$, $p = 6.25 \times 10^{-7}$; Fig. 5); this is consistent with Brooks's (2004) finding that stronger tornadoes are generally larger.

Despite structural differences in the updraft characteristics revealed in Fig. 4, all TLVs within these simulations are associated with significant rotating updrafts, especially at low levels. We find, however, that low-level (1.5 km) updraft intensity has only a modest correlation with peak TLV intensity ($R^2 = 0.41$, $p = 4.1 \times 10^{-5}$; Fig. 6), thus suggesting that although a strong, low-level updraft may be necessary for TLV formation, low-level updraft strength alone does not sufficiently explain TLV intensity. This result is expected, considering that low-level vertical stretching ($\partial\zeta/\partial t \sim \zeta\partial w/\partial z$) is dependent not only on the magnitude of the low-level w, but also on the availability of near-surface ζ that can be stretched and intensified by the vertical velocity gradient, as well as on the length of time near-surface ζ undergoes this stretching. The correlation between the 3 and 6 km updraft intensity and TLV intensity are lower ($R^2 = 0.34$, $p = 3.2 \times 10^{-2}$; $R^2 = 0.13$, $p = 3.9 \times 10^{-2}$), with the midlevel updraft intensity appearing to have little relation to peak TLV intensity. The pretornadic peak w at all levels is also relatively uncorrelated to the TLV intensity (not shown). Consistently, Trapp et al. (2017) also found that the pretornadic updraft intensity in supercells was relatively uncorrelated to TLV intensity.

Also consistent with Trapp et al. (2017) is a positive correlation between low-level (1.5-km) mesocyclone area and TLV intensity at the pretornadic stage as well as in the 15-min period preceding peak intensity, respectively ($R^2 = 0.45$, $p = 1.31 \times 10^{-5}$; $R^2 = 0.61$, $p = 5.23 \times 10^{-8}$; Fig. 7). These correlations are, however, significantly weaker using the 3 km ($R^2 = 0.06$, $p = 0.17$; $R^2 = 0.22$; $p = 4.8 \times 10^{-3}$) and 6 km ($R^2 = 0.03$, $p = 0.35$; $R^2 = 0.30$, $p = 8.1 \times 10^{-4}$) mesocyclone area. Thus, the low-level mesocyclone area, and therefore low-level mesocyclone width, appears to serve as a control for TLV intensity within QLCSs, although the control is not as straightforward as in supercells (Trapp et al. 2017).

The hypothesized intensity control does not appear to depend on the convection initiation mechanism in the simulations, given that the respective TLVs produced in the UG and LF experiments do not differ substantially in their intensity, with average peak TLV vertical vorticity of 0.178 and 0.164 s^{-1}, respectively. However, the LF QLCSs produced nearly twice as many TLVs per QLCS than the UG QLCSs, with 21 of the 34 total TLVs associated with the three LF simulations. This is likely attributable, in part, to the presence of a supercell ahead of the southern portion of the QLCS in two of the UG simulations, which appears to disrupt the QLCS inflow, leading to weaker convective development in these areas of the QLCSs (Fig. 8). The QLCSs in UG, quarter-circle hodograph simulations develop one distinct bowing segment with strong w, while the LF QLCSs develop two. As has been previously shown (e.g., Funk et al. 1999), these bowing segments are associated with the recurring development of (relatively) deep mesocyclones and repeated tornadogenesis, both of which tend to occur at the northern apex of the bows, though can form in multiple locations within the bow. With only one such bowing segment forming in the UG simulation, fewer favored locations for tornadogenesis develop, and as a result, fewer TLVs form.

In general, the most intense TLVs resulted from QLCSs simulated in environments with hodograph curvature (Table 2). Indeed, the eight strongest TLVs were produced in environments with quarter-circle hodographs and thus relatively larger SRH. This result corresponds well to climatological studies of QLCS tornadoes and their environments, which show that higher EF ratings are generally associated with environments characterized by larger SRH (e.g., Smith et al. 2012). In our simulations, the apparent dependence of TLV intensity on hodograph curvature is likely related to the relative persistence of the TLVs in the environments with curved versus straight hodographs: for reasons explored later, the mean and median durations of TLVs in experiments with curved hodographs are 15.5 and 10 min, respectively, while such durations in experiments with straight hodographs are 12 and 7.5 min, respectively (Fig. 9). This difference is even more pronounced excluding the longest duration events (a significant outlier for the straight hodograph TLVs) for each, giving respective mean durations of approximately 14 and 8.5 min.

Additionally, more numerous TLVs also resulted from QLCSs simulated in environments with larger magnitudes of 0–1 km bulk shear (Table 2), in line with previous findings that mesovortex production within QLCSs is closely related to low-level shear magnitude (e.g., Trapp and Weisman 2003;

TABLE 2. Details of tornado-like vortices (TLVs) analyzed. Storm-relative helicity (SRH) values are calculated using approximate QLCS motion.

TLV ζ_{max}	Simulation name	Hodograph shape	Initiation mechanism	0–1 km bulk shear (m s^{-1})	0–3 km bulk shear (m s^{-1})	0–1 km SRH (m^2 s^{-2})	0–3 km SRH (m^2 s^{-2})
0.35	QCHSLF	Quarter circle	Linear forcing	17	35	161	342
0.3	QCLS	Quarter circle	Upscale growth	14	29	266	470
0.226	QCHSLF	Quarter circle	Linear forcing	17	35	161	342
0.222	QCLS	Quarter circle	Upscale growth	14	29	266	470
0.22	QCHSLF	Quarter circle	Linear forcing	17	35	161	342
0.211	QCHSLF	Quarter circle	Linear forcing	17	35	161	342
0.21	QCLSLF	Quarter circle	Linear forcing	14	29	265	478
0.208	QCHS	Quarter circle	Upscale growth	17	35	170	385
0.206	STRLS	Straight	Upscale growth	10	29	103	308
0.201	QCHS	Quarter circle	Upscale growth	17	35	170	385
0.174	STRLSLF	Straight	Linear forcing	10	29	120	360
0.172	QCLSLF	Quarter circle	Linear forcing	14	29	265	478
0.17	QCHS	Quarter circle	Upscale growth	17	35	170	385
0.169	STRLSLF	Straight	Linear forcing	10	29	120	360
0.167	QCHS	Quarter circle	Upscale growth	17	35	170	385
0.167	QCHS	Quarter circle	Upscale growth	17	35	170	385
0.166	STRHS	Straight	Upscale growth	12	35	44	131
0.155	STRLS	Straight	Upscale growth	10	29	103	308
0.149	STRLSLF	Straight	Linear forcing	10	29	120	360
0.149	STRLSLF	Straight	Linear forcing	10	29	120	360
0.146	QCHSLF	Quarter circle	Linear forcing	17	35	161	342
0.141	STRLSLF	Straight	Linear forcing	10	29	120	360
0.14	QCLSLF	Quarter circle	Linear forcing	14	29	265	478
0.133	QCLSLF	Quarter circle	Linear forcing	14	29	265	478
0.127	STRLSLF	Straight	Linear forcing	10	29	120	360
0.126	QCHSLF	Quarter circle	Linear forcing	17	35	161	342
0.125	QCHSLF	Quarter circle	Linear forcing	17	35	161	342
0.123	STRLS	Straight	Upscale growth	10	29	103	308
0.122	STRHS	Straight	Upscale growth	12	35	44	131
0.122	QCHSLF	Quarter circle	Linear forcing	17	35	161	342
0.122	QCHSLF	Quarter circle	Linear forcing	17	35	161	342
0.121	QCLSLF	Quarter circle	Linear forcing	14	29	265	478
0.118	STRLSLF	Straight	Linear forcing	10	29	120	360
0.116	QCHS	Quarter circle	Upscale growth	17	35	170	385

Weisman and Trapp 2003). Note, however, that the number of TLVs may be impacted by TLV duration, with longer-lived TLVs potentially decreasing the total number produced by the QLCS.

TLV persistence and intensity appear to be linked to the cold pool characteristics of each QLCS. Indeed, examining cross sections of the updrafts and cold pools associated with strong TLVs in environments characterized by curved and straight hodographs (Fig. 10), we find that the cold pool in the straight hodograph case is, on average, deeper and stronger. In contrast, the shallower and weaker cold pool in the curved hodograph case allows for more persistent updraft forcing locally. The straight hodograph–deep cold pool linkage is explained in part by the association of this environment with more numerous, larger QLCS updrafts (not shown). In supercells, larger updrafts have been shown to result in larger downdrafts that, in turn, generate stronger, deeper cold pool (Marion and Trapp 2019). The curved hodograph–shallow cold pool linkage is likely due to the stronger low-level (0–1 km) vertical wind shear associated with the curved hodograph

(Table 2). Specifically, the stronger low-level shear should result in greater vertical mixing at the top of the cold pool, reducing its depth and intensity (Marion and Trapp 2019).

The combined influences of the environmental wind shear and cold pool characteristics have also been shown to affect QLCS updraft tilt (Rotunno et al. 1988), and updraft tilt in turn may provide a means to discriminate nontornadic from tornadic updrafts (e.g., Schaumann and Przybylinski 2012). By extension, this suggests that updraft tilt may also impact QLCS tornado intensity, with more upright updrafts being associated with deeper, more persistent rotation, leading to more intense vortices with longer periods of stretching of near-ground vertical vorticity. The "uprightness" of an updraft can be quantified in the 15 min period prior to peak TLV intensity by calculating the horizontal distance between the locations of the maximum w at two different altitudes, namely, the 0.875 km (cloud base) and 2 km levels, with the minimum distance during this period being the minimum updraft tilt. These levels are chosen because a mesocyclone as defined above existed at each of these levels for every TLV; however, in many of the cases,
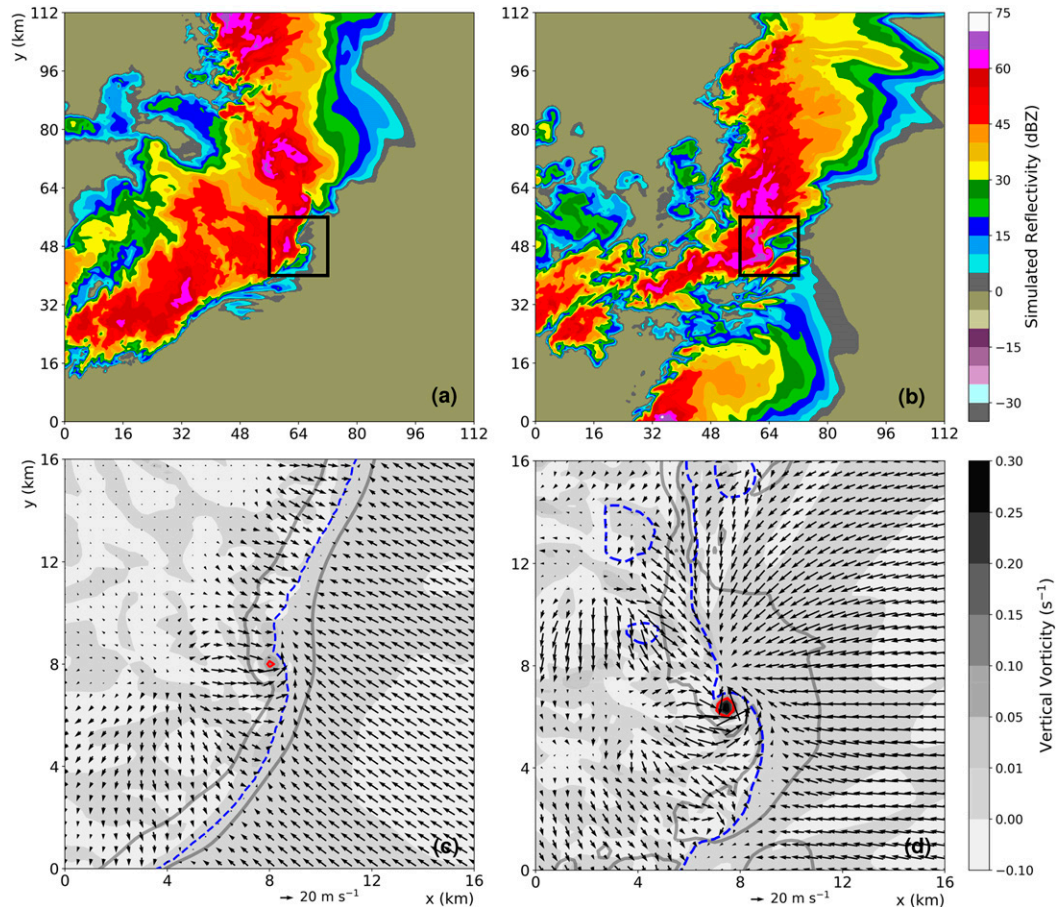
FIG. 4. Horizontal cross sections of (a),(b) 1.25 km simulated reflectivity (dBZ; filled contours), and (c),(d) horizontal cross sections of near-surface (67.5 m) vertical vorticity (s^{-1}; filled contours), near-surface perturbation potential temperature (-1 K; dashed blue contour), 1.25 km vertical velocity (10 m s^{-1}; gray contour), and near-surface Okubo–Weiss parameter (10^{-2} s^{-2}; red contour) for (a),(c) low-end (QCLSLF; see Table 2) and (b),(d) high-end (QCLS; see Table 2) tornado-like vortices (TLVs). The black squares in (a) and (b) outline the areas shown in (c) and (d).

we note the storm updraft extended below cloud base and above 2 km. Based on this quantification, we find, rather surprisingly, that TLV intensity is poorly correlated ($R^2 = 0.06$) to the minimum tilt of the low-level updraft (Fig. 11). Performing the same analysis over a deeper layer, such as cloud base to 3 km, does not yield much improved results ($R^2 = 0.11$). Overall, most (~82%) of the updrafts associated with vortices meeting our TLV criteria have relatively little tilt (<2 km) in the low levels. As such, an upright updraft may be required for TLV formation, but the amount of updraft tilt appears to have little impact on TLV intensity in these simulations.

It is possible that a consideration of null cases is necessary to reveal an impact of updraft tilt on TLV intensity. Here, we equate "null" with "near-tornadic," and identify such near-TLVs by requiring peak near-surface OW between 5×10^{-3} (50% of TLV OW) and 10^{-2} s^{-2}. Like the TLVs identified above, an association with a low-level updraft is also required for near-TLVs. Only two such vortices are identified within these simulations, so a robust statistical analysis using these vortices is not possible. Nonetheless, no difference

is discernable between the near-TLV intensity and TLV updraft tilt and depth. Additionally, both the low-level mesocyclone area and low-level updraft w associated with these near-TLVs are comparable to those of the lowest-end TLVs.
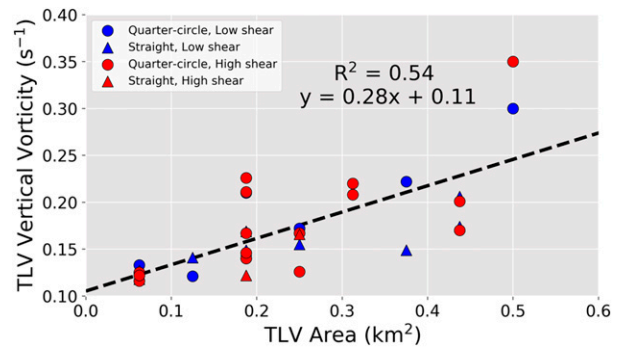

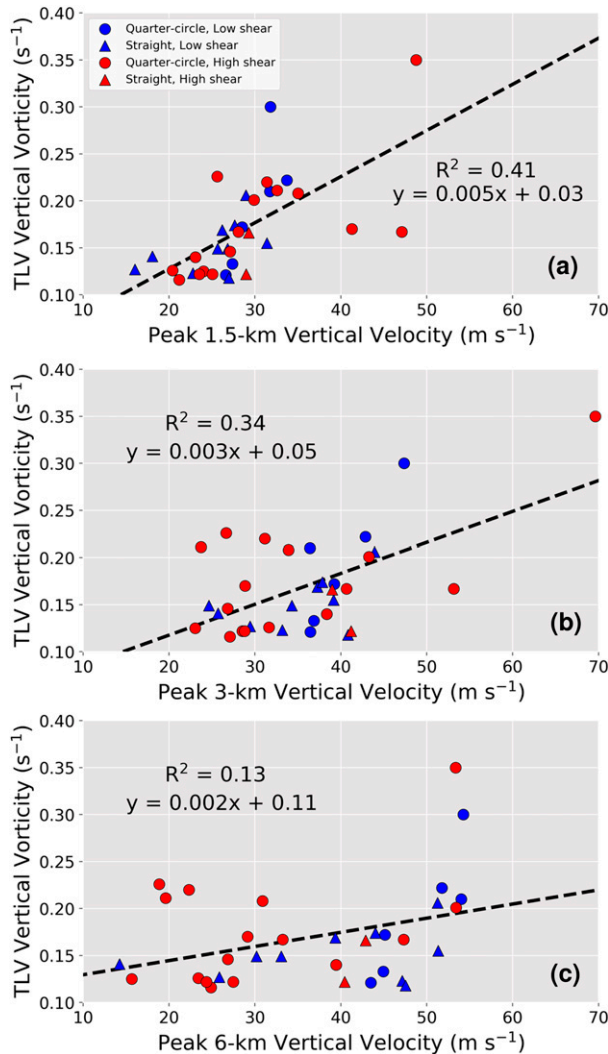FIG. 5. Scatterplot of TLV horizontal area (km^2) and peak TLV vertical vorticity (s^{-1}).

FIG. 6. Scatterplots of (a) 1.5, (b) 3, and (c) 6 km peak updraft vertical velocity (m s^{-1}) during 15-min period prior to peak vortex intensity, and peak vertical vorticity (s^{-1}).
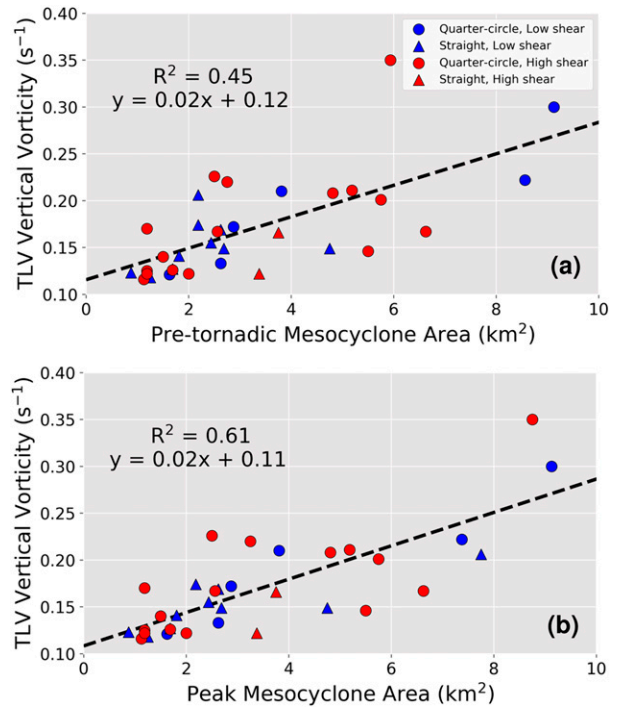

FIG. 7. Scatterplots of 1.5 km mesocyclone horizontal area (km^2) during (a) 15 min period prior to peak vortex intensity and (b) 15 min period prior to peak vortex intensity, and peak vertical vorticity (s^{-1}).

dynamics. The resultant contribution of the buoyancy forcing to vertical acceleration is given by

$$\left.\frac{Dw}{Dt}\right|_B = -\frac{1}{\overline{\rho}}\left(\frac{\partial p'_B}{\partial z}\right) + B, \tag{1}$$

where $\overline{\rho}$ denotes the model base-state density, and the right-side terms are the vertical buoyancy pressure gradient force and thermal buoyancy (B), respectively. The buoyancy perturbation pressure is determined through

$$\nabla^2 p'_B = \frac{\partial(\overline{\rho}B)}{\partial z} \tag{2}$$

and is calculated herein without the (negative) contributions of precipitation loading; however, the difference between the buoyancy pressure within the updraft, with and without precipitation loading, is generally less than 15% (not shown).

The resultant contribution of the (total) dynamics forcing to vertical acceleration is given by

$$\left.\frac{Dw}{Dt}\right|_D = -\frac{1}{\overline{\rho}}\left(\frac{\partial p'_D}{\partial z}\right), \tag{3}$$

where the dynamics perturbation pressure is determined through

$$\nabla^2 p'_D = -2\overline{\rho}\mathbf{S}\cdot\nabla_H w - \overline{\rho}\left[\left(\frac{\partial u'}{\partial x}\right)^2 + \left(\frac{\partial v'}{\partial y}\right)^2 + \left(\frac{\partial w'}{\partial z}\right)^2\right]$$
$$- \frac{d^2\ln\overline{\rho}}{dz^2}w^2\right] - 2\overline{\rho}\left(\frac{\partial v'}{\partial x}\frac{\partial u'}{\partial y} + \frac{\partial w'}{\partial x}\frac{\partial u'}{\partial z} + \frac{\partial w'}{\partial y}\frac{\partial v'}{\partial z}\right), \tag{4}$$

As implied in the stretching argument invoked above, the other updraft characteristic besides tilt that may also relate to QLCS tornado intensity is depth. Compared to the supercells examined by Trapp et al. (2017), the QLCS rotating updrafts associated with strong TLVs here have similar depth to those of supercells (Fig. 12) (see also Trapp and Weisman 2003; Weisman and Trapp 2003; Atkins and St. Laurent 2009a,b). The width of the mesocyclones shown in Fig. 12, however, follow the findings above—namely, the wider mesocyclones produce the stronger TLVs. As such, it appears that mesocyclone width, irrespective of storm mode, may correspond to potential tornado intensity.

To understand the forcings and, by extension, vertical accelerations that ultimately result in the differences in updraft characteristics, we follow Rotunno (1985) and others and decompose the pressure into contributions from buoyancy and
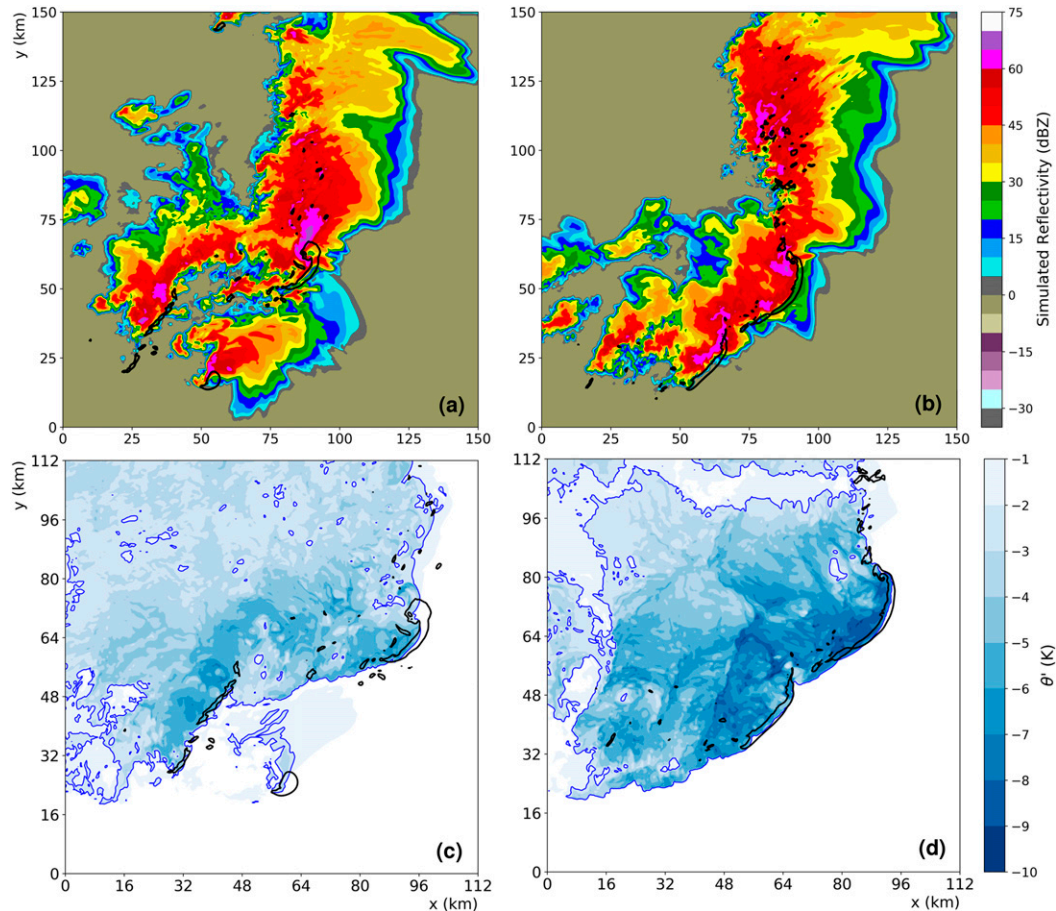
FIG. 8. Horizontal cross sections of (a),(b) 1.25 km simulated reflectivity (dBZ; filled contours) and 1.5 km vertical velocity (10 m s^{-1}; black contour), and near-surface (67.5 m) cold pool potential temperature perturbation (θ'; K; filled contours) with $\theta' = -2$ K highlighted (blue contours) for quarter-circle hodograph (a),(c) upscale growth (QCLS; see Table 2) and (b),(d) linearly forced (QCLSLF; see Table 2) cases at $t = 4$ h.

where **S** is the environmental shear vector [**S** $= (dU/dz, dV/dz, 0)$], u' and v' are the perturbation horizontal velocity components relative to the model base state, the first rhs term represents the contribution of the linear dynamics to the perturbation pressure, and the second and third rhs terms represent the contribution of the nonlinear dynamics to the perturbation pressure.

The following analysis is focused on four QLCS TLVs in addition to a supercell TLV ($\zeta_{max} = 0.2$ s^{-1}) for comparison (see Fig. 12). The QLCS TLV cases are selected to represent the spectrum of QLCS TLV intensities observed in these simulations, with TLV ζ_{max} varying from 0.133 to 0.3 s^{-1}. Vertical profiles of the average positive buoyancy and dynamics forcings within a 7.5 × 7.5 km^2 box centered on the near-surface ζ_{max} are shown in Fig. 13 for the updraft associated with each TLV, 5 min prior to the formation of the TLV. This analysis reveals that, for each case, the average low-level dynamics forcing of upward vertical accelerations is much larger (~2–3 times) than the buoyancy forcing. In two of the QLCS cases (Figs. 13c,d) and the supercell (Fig. 13e) case, the buoyancy forcing is maximized in the midlevels, as expected due to the contribution of the thermal

buoyancy; the updrafts in both cases are associated with a single, deep core of buoyancy forcing (not shown). In the lower-end QLCS updrafts (Figs. 13a,b), however, the buoyancy forcing is maximized at relatively lower levels.

The dynamics forcing in the QLCS cases is maximized in the low levels, while in the supercell case, forcing maxima at low and midlevels are present. Based on calculations of the right-hand side of Eq. (4) (not shown), the midlevel forcing maximum of the supercell updraft is primarily associated with the toroidal circulation contribution [i.e., $(\partial w/\partial x)(\partial u'/\partial z) + (\partial w/\partial y)(\partial v'/\partial z)$] to the dynamics pressure, which has been previously found to be primarily associated with new updraft development and updraft widening (e.g., Marion and Trapp 2019). The midlevel dynamics forcing of the QLCS updrafts shares some similarities with that of the supercell—namely, it is distributed over a deep layer extending from near cloud-base to the midlevels, and also benefits from the "spin" contributions to the dynamics pressure [i.e., third term, right-hand side of Eq. (4)]. The strength of this forcing relative to that at low levels, however, is less than that of the supercell updraft.
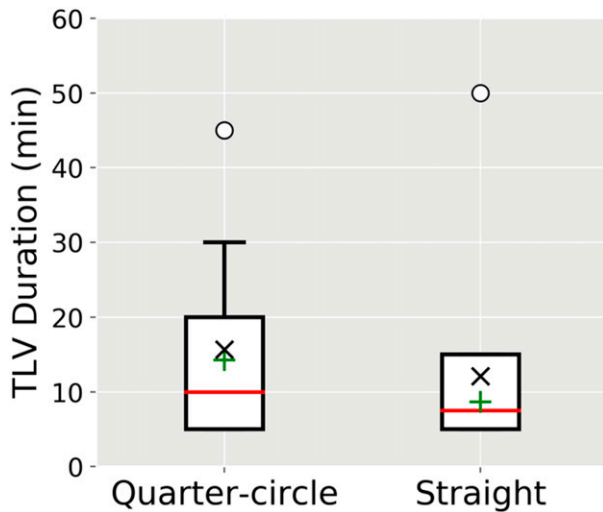
FIG. 9. Box-and-whisker plot of TLV duration for environments with shear profiles characterized by quarter-circle and straight hodographs. Mean TLV duration including and excluding the longest-lasting TLV are indicated by the black × and green plus sign, respectively.

FIG. 10. Vertical cross sections (x direction) of potential temperature perturbation (θ'; K; filled contours) and $10 \, \mathrm{m \, s^{-1}}$ updraft vertical velocity (black contours) for (a) quarter-circle (QCLS; see Table 2) and (b) straight (STRLS; see Table 2) hodograph simulations. Cross sections are taken through the strongest portion of the low-level (1.5 km) updraft at the time of peak TLV intensity.

The low-level forcing of the weakest QLCS updrafts is weaker than both the higher-end QLCS and supercell updrafts; however, the other QLCS updrafts have low-level forcings comparable to or greater than that of the supercell updraft. Despite the weaker updraft forcing, the supercell TLV reaches an intensity greater than two of the QLCS TLVs. So, if the low-level forcings associated with the supercell updraft is weaker than that of the QLCS updrafts, a question remains as to why the supercell TLV reached greater intensity than some of the QLCS TLVs.

Based again on calculations of Eq. (4), the difference in low-level updraft forcing between the supercell and QLCS cases owes mostly to the horizontal convergence contribution [i.e., $(\partial u'/\partial x)^2 + (\partial v'/\partial y)^2$] to the dynamics pressure. The layer of strong low-level convergence and, therefore, low-level dynamics forcing in the QLCS is caused, to some extent, by its relatively strong and deep cold pool. Similar dynamics have been suggested to impact supercell low-level mesocyclone strength (Houston 2017); however, the magnitude of the convergence owing to the supercell cold pool is likely to be much less than that of the QLCS, with a QLCS producing a deeper, stronger cold pool. With the maximum in the dynamics forcing in the low levels of the QLCS, however, the QLCS updraft may be more dependent on the buoyancy forcing to counteract the dynamically driven downward directed perturbation pressure gradient force above the low-level forcing maximum, which acts to diminish the updraft and near-surface vortex.

As alluded to earlier, the effects of the cold pool are actually twofold. While the low-level convergence associated with the outflow contributes positively to low-level vertical accelerations, causing stronger vertical motion at the gust front and resulting in stronger near-surface vortex development, the relatively stronger outflow with a strong, deep cold pool may also disrupt the intensification of near-surface and even low-level updraft
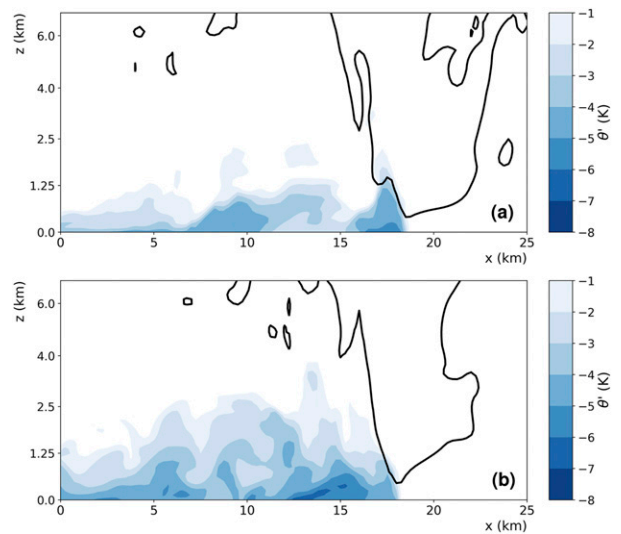
rotation. In other words, the stronger and deeper layer of outflow may contribute to limiting TLV intensification. This can be demonstrated using a simplified version of the vertical vorticity tendency equation,

$$\frac{\partial \zeta}{\partial t} \approx -\mathbf{v}_H \cdot \nabla \zeta + \zeta \frac{\partial w}{\partial z} + \boldsymbol{\omega} \cdot \nabla w, \qquad (5)$$

where the first rhs term represents horizontal advection, the second rhs term represents stretching, and the last rhs term represents tilting, which are sufficient to satisfy our interest in the near-surface outflow. Here, the two TLVs shown in Figs. 4, 13a, and 13d are examined as representative low-end and high-end TLVs. The rhs terms of Eq. (5) are computed in a $10 \times 10 \, \mathrm{km^2}$ box, roughly twice the width of the minor axis of the low-end TLV updraft, centered on the near-surface vertical
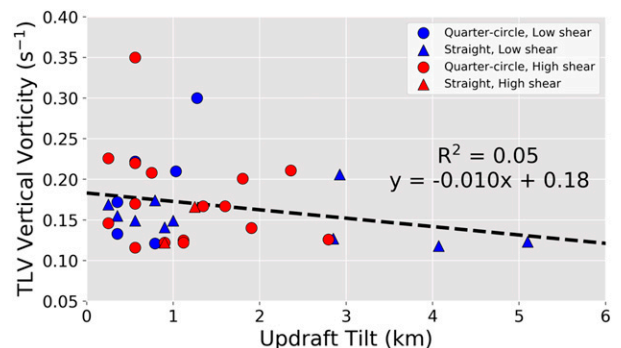

FIG. 11. Scatterplot of the minimum horizontal distance between vertical velocity (w; $\mathrm{m \, s^{-1}}$) peaks at cloud base (875 m) and 2 km and peak TLV vertical vorticity ($\mathrm{s^{-1}}$).
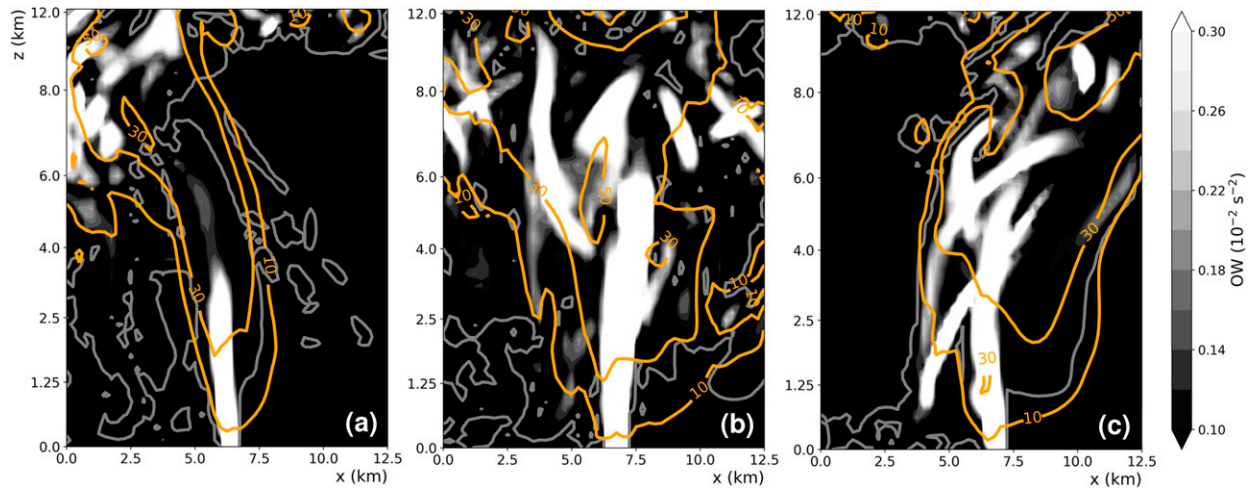
FIG. 12. Composite (y direction) vertical cross section (x direction) of vertical velocity (m s^{-1}; orange contours) and Okubo–Weiss parameter (OW; s^{-2}; filled contours), with mesocyclonic OW highlighted (gray contours) for a (a) low-end tornadic QLCS updraft (QCLSLF; see Table 2), (b) high-end tornadic QLCS updraft (QCLS; see Table 2), and (c) supercell updraft (QCLS; see Table 2). Composites are generated using maximum values of each quantity within 2 km of the near-surface vertical vorticity maximum.

vorticity maximum. The horizontal mean of grid points where the magnitude of the tendency contribution exceeds 10^{-4} s^{-2} (the approximate 5th- and 95th-percentile values) is computed at each vertical level within the box. Using this threshold eliminates grid points largely outside the area of interest (i.e., in front of the QLCS gust front), which heavily bias the resulting mean toward low-magnitude values.

These computations are performed over a time period beginning 5 min prior to TLV formation to TLV dissipation, building a time series of the vertical vorticity tendency throughout the lifetime of the TLV (Fig. 14). For the high-end case during intensification, the advection term is near-zero. This term becomes largely negative near the time of peak intensity. Following this, the stretching contribution to the vertical vorticity tendency decreases significantly, in part due to the reduction in near-surface vertical vorticity. The updraft is also disrupted by the strong, deep outflow. This is best illustrated using vertical profiles of the vertical vorticity tendency (Fig. 15). During TLV intensification, the stretching profile is largely positive throughout the low levels of the storm (Fig. 15a). Soon after the enhancement of the outflow, however, the stretching contribution to the vertical vorticity becomes largely near-zero and, at times, negative within the low levels, ultimately contributing to a negative vertical vorticity tendency above ~250 m (Fig. 15b).

For the low-end TLV, the contribution from horizontal advection is negative prior to peak intensity, indicating relatively strong outflow prior to this TLV is forming (Fig. 14). When the advection contribution becomes less strongly negative near the surface, the TLV forms. Strong outflow then disrupts the near-surface vortex, resulting in a weakening of the near-surface vortex below the TLV criteria 5 min after its formation. Despite a strong positive contribution from stretching, the TLV struggles to form and intensify because of the strongly negative advection contribution. Further, although the peak

vertical vorticity tendency in this case is stronger in the low-end TLV than the example high-end TLV, the low-end TLV does not persist over a similar time scale and, thus, does not reach a greater intensity. We note, however, that the updraft is not disrupted as it is in the high-end case (not shown), with only the surface vertical vorticity tendency significantly impacted by the strengthening outflow, which allows the updraft to continue on, aiding in the development of a new TLV 10 min later.

The two adverse impacts of the cold pool can thus be identified as the negative horizontal vorticity advection that results from outflow intensification (equated here to the colloquialism "gusting out") as well as the potential for the low-level updraft forcing (i.e., "undercutting"), which results in a weaker, or even negative, contribution due to stretching. Even if both occur, however, the vertical vorticity associated with the mesovortex and TLV can live on, ultimately supporting to the development of new TLVs. This appears to be more likely if the low-level vortex but not the updraft is affected by the outflow, as if both occur, a new updraft must form to take advantage of the pre-existing vortex.

Overall, it is the deleterious impacts of the QLCS cold pool that contribute to the generally intermittent nature of the QLCS mesocyclones. Note that long-lived updrafts do exist within the QLCSs, particularly those associated with bowing segments. As with the mesovortices and mesocyclones identified by Funk et al. (1999), deeper mesocyclones tend to form at the apex of these bowing segments. While the broader updraft may persist for long periods of time (>1–2 h), these rotating updraft cores tend to dissipate on shorter time scales, usually after being separated from the broader area of ascent ahead of the bow (Fig. 16). This behavior has been previously noted by Trapp and Weisman (2003), who found that new mesovortices often developed at the new ends of these segments or within new segments entirely. Consistent with their findings, the repeated generation of new rotating updraft cores within the
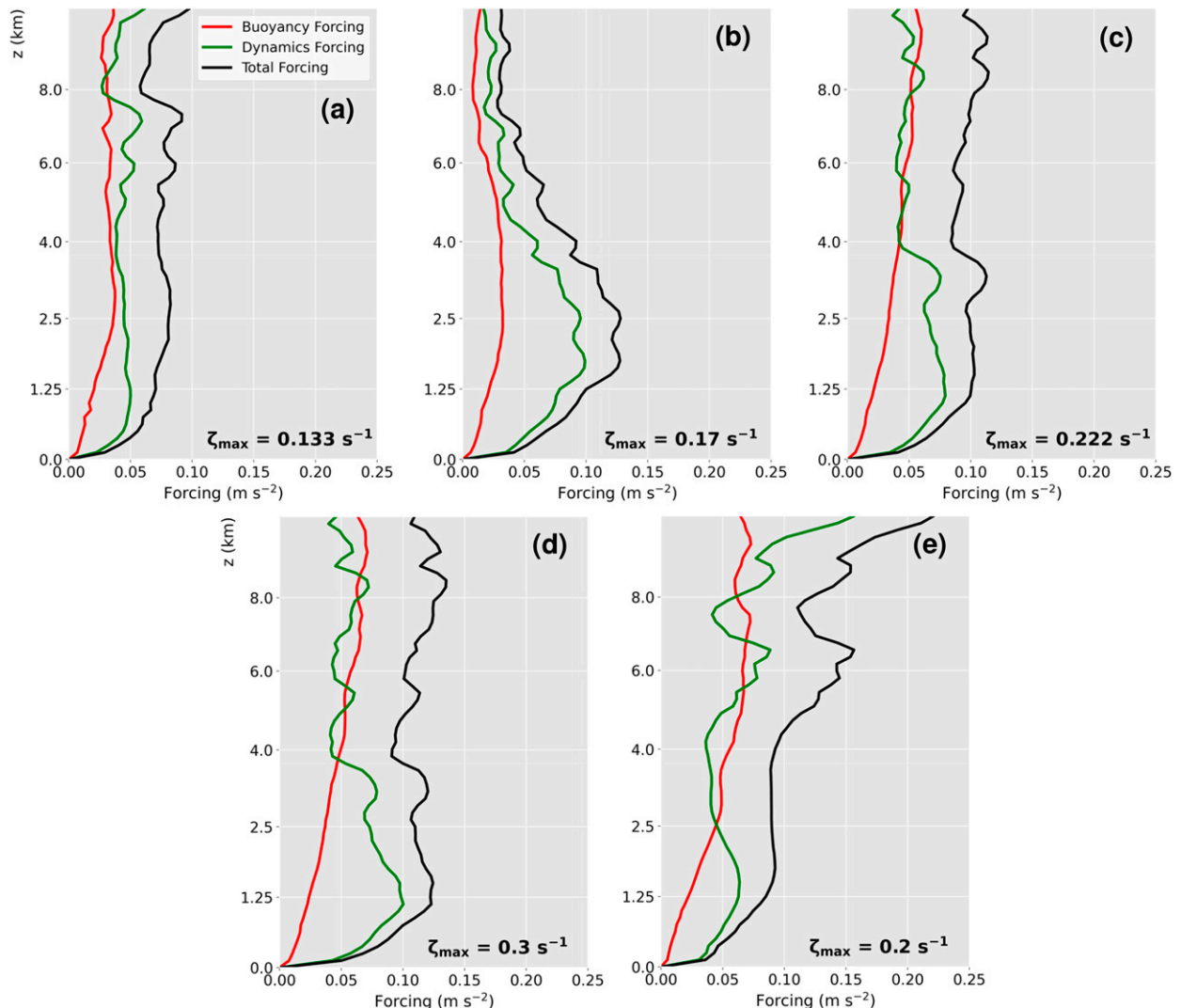
FIG. 13. Vertical profiles of average positive buoyancy (red), dynamics (green), and total (black) forcings (m s^{-2}) for (a)–(d) quasi-linear convective system (QLCS) and (e) supercell updrafts 5 min prior to TLV formation. Note that the y axis (z) does not increase linearly with height, with increased resolution in the low levels.

larger updraft leads to fluctuations in the magnitude of the updraft vertical velocity and rotation over time.

To demonstrate this, three supercell updrafts and three bowing segment updrafts within the same simulations are examined through a quantification of the maximum 1.5 km w and updraft helicity (UH) for each updraft type every 5 min over the same time period (>1.5 h in each case—the lifetime of the QLCS updraft). The standard deviation (σ) both of w and UH are, on average, much greater within the QLCS updrafts relative to the supercell updraft (increase of 48% and 117%, respectively; see Table 3). With larger σ_w and σ_{UH}, it appears that the QLCSs, relative to supercells, struggle to maintain deep, rotating updrafts, consistent with previous findings (e.g., Trapp et al. 1999). As follows, a persistent source of stretching of the near-surface vortex may be difficult to develop, so the large low-level SRH values associated with QLCS tornado

environments may be necessary to increase the likelihood of tornado formation, particularly strong tornadoes, through their contribution to low-level updraft rotation persistence and, by extension, low-level vertical accelerations.

Finally, though previous studies have noted the development of tornadoes in association with "embedded supercells" (e.g., French and Parker 2012; Smith et al. 2012), we consider the rotating QLCS updrafts identified within these simulations to be different than supercellular updrafts. This is clearly demonstrated by the differences in kinematic structure (Fig. 4) and forcing (Fig. 13). This is further demonstrated by updraft motion. We define the location of the QLCS and supercell updrafts as the centroid of the 10 m s^{-1} w contour, and we define the location of the QLCS as the centroid of the largest 45 dBZ simulated reflectivity object at 1 km altitude. For the supercell motion vector, the storm motion is averaged over an
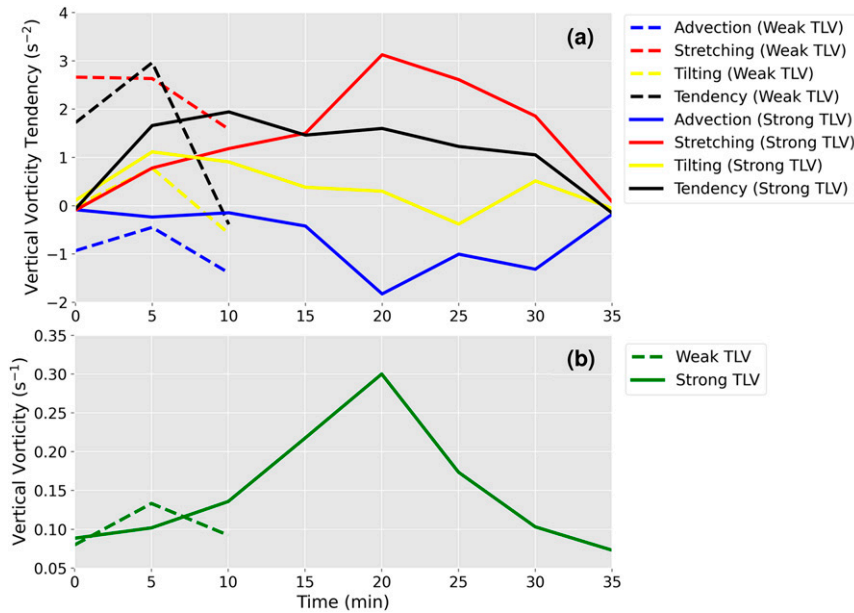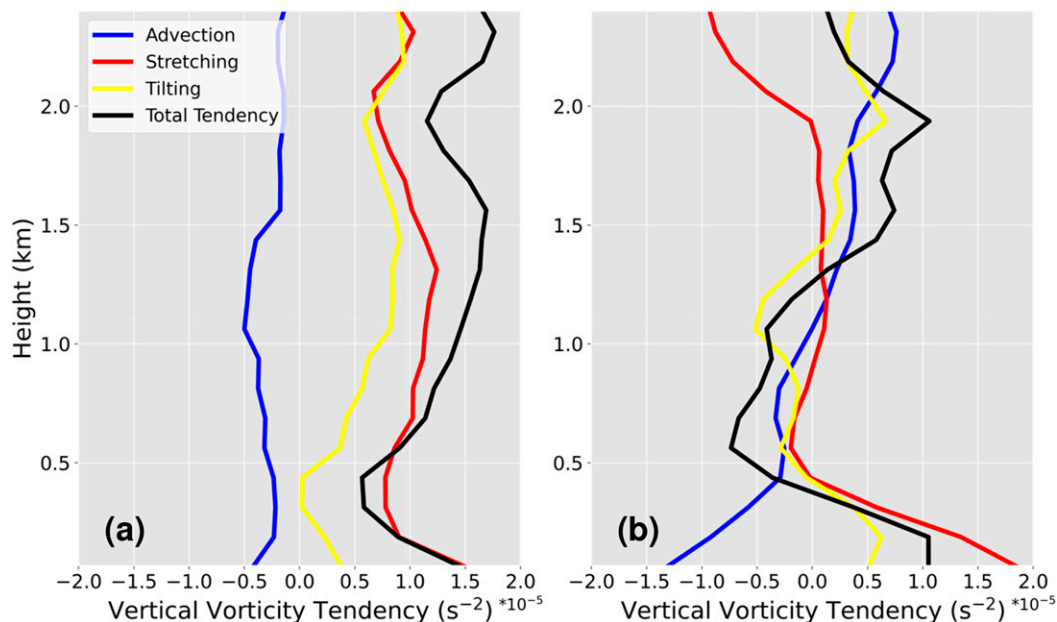
FIG. 14. (a) Time series of the vertical vorticity tendency (s^{-2}) contributions due to horizontal advection (blue), stretching (red), tilting (yellow), and total tendency (black), and (b) time series of the vertical vorticity (green) for high-end (solid) and low-end (dashed) TLVs for time period from 5 min prior to TLV formation to TLV dissipation.

hour period; for the rotating QLCS updrafts, the storm motion is averaged over the lifetime of the rotating updraft core (<60 min). Comparing the motion vectors of a supercell and two rotating QLCS updrafts within a simulation, we find that the speed of the QLCS updrafts is roughly 50% faster than that

of the supercell (Fig. 17). The motion of these updrafts is more comparable to that of the QLCS itself, indicating that the motion of the individual rotating updrafts is likely resulting from similar processes as the system (i.e., primarily cold pool driven). Moreover, these QLCS mesocyclones

FIG. 15. Vertical profiles of the vertical vorticity tendency (s^{-2}) contributions due to horizontal advection (blue), stretching (red), tilting (yellow), and total tendency (black) for high-end TLV storms during TLV (a) intensification and (b) dissipation.
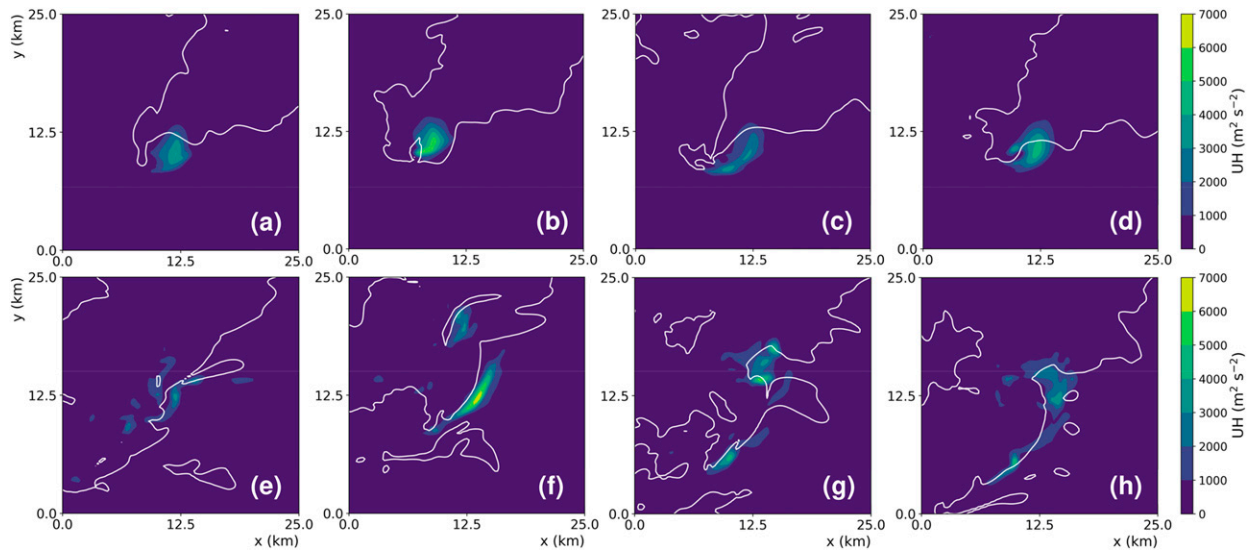
FIG. 16. Updraft helicity (filled contours; $m^2\,s^{-2}$) and simulated reflectivity (white contours; 40 dBZ) for (a)–(d) supercell and (e)–(h) QLCS updrafts at $t =$ (a),(e) 3, (b),(f) 3.5, (c),(g) 4, and (d),(h) 4.5 h from the QCLS simulation.

develop spontaneously within the system, with no dependence on the preceding supercellular convective mode, such as might be found with supercells that are overtaken by a convective line and become embedded while maintaining some of their initial supercellular characteristics (e.g., as shown in French and Parker 2012). Because of these factors, we hesitate to call these updrafts supercellular in nature. The low-level dynamics near the time of tornado formation appear to be somewhat similar those observed in supercells, with the development of significant low-level updraft rotation prior to tornado formation; however, as noted within the discussion of the pressure decomposition, some of the low-level forcing is supplied by the QLCS cold pool.

4. Conclusions and future work

This study is motivated by observational data showing that QLCS tornadoes rarely have enhanced Fujita ratings of EF-3 and higher (Smith et al. 2012) and, thus, by a desire to understand the limits on QLCS tornado intensity. Using idealized numerical model simulations of QLCSs, we find that QLCS TLV intensity is controlled in part by the area of the low-level mesocyclone in which the TLV forms. This basic result is consistent with the theoretical reasoning expressed in Trapp et al. (2017), which was derived from Kelvin's circulation theorem as applied specifically to supercells. In agreement with the analysis of Doppler radar data by Sessa and Trapp (2020), the relative weakness of observed and simulated QLCS tornadoes appears to be due in part to the relatively smaller size of QLCS low-level mesocyclones. The relationship between mesocyclone area and tornado intensity is weaker for QLCSs than for supercells (Sessa and Trapp 2020), however, suggesting the existence of modulating factors in QLCSs. This factor is time, or more precisely, the lack of persistency in deep rotating updrafts, such as is reflected in the short relative lifetime of

mesocyclonic updraft cores in QLCSs as compared to supercells. The primary contributor to this lack of persistency is the QLCS cold pool and associated dynamics.

Indeed, analyses performed herein of the decomposed forcings of vertical accelerations confirm the role of the QLCS cold pool in driving low-level updraft development, and also confirm that the differences in the deep updraft characteristics and low-level updraft forcings between supercells and QLCSs are attributable to the QLCS cold pool. The cold pool, however, may also serve to limit rotating updraft and TLV longevity, ultimately inhibiting QLCS TLV intensification.

In contrast to the area and persistency of low-level mesocyclones, peak updraft speed nor low-level updraft tilt tended not to be good predictors of QLCS TLV intensity; further analysis is required to determine why. Note, however, that the majority of TLVs formed beneath relatively upright updrafts, which is consistent with previous findings that suggest that upright updrafts may be favored locations of QLCS tornadogenesis (e.g., Schaumann and Przybylinski 2012). Nonetheless, all TLVs herein form beneath rotating

TABLE 3. Comparison of the time variability of vertical velocity (w; m s^{-1}) and updraft helicity (UH; m^2 s^{-2}) for supercell and QLCS updrafts.

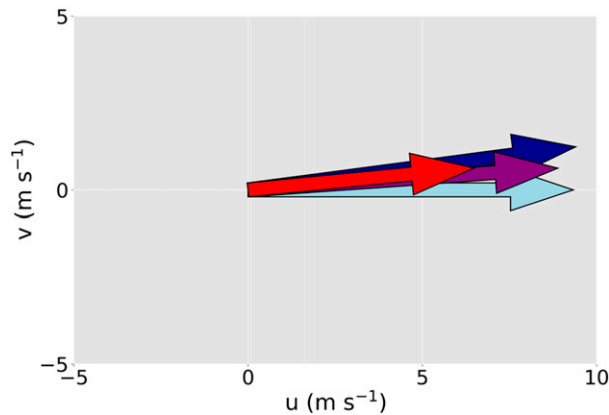| Mode (case)	σ_w	σ_{UH}
Supercell (QCLS)	2.30	772
Supercell (QCHS)	3.19	702
Supercell (QCHSLF)	1.76	340
Supercell (average)	2.42	605
QLCS (QCLS)	2.54	124
QLCS (QCHS)	5.41	1720
QLCS (QCHSLF)	2.82	992
QLCS (average)	3.59	1317

FIG. 17. Storm motion vectors for example supercell (red), QLCS (purple), and rotating QLCS updrafts (dark and light blue) from the QCLS (see Table 2) simulation.

updrafts, and accordingly, rotating QLCS updraft cores appear to serve as good indicators of favored locations for tornadogenesis, which is consistent with previous findings (e.g., Atkins et al. 2004; Schaumann and Przybylinski 2012). Unsurprisingly, the environments characterized by higher low-level SRH also tended to produce the strongest, longest-lived TLVs, as noted in tornado climatology (e.g., Thompson et al. 2012). It also appears as if the conditions favorable for the development of a large low-level mesocyclone, namely, large environmental vertical wind shear over the 0–1 km layer, are also conducive to the development of significant near-surface vertical vorticity, similar to previous studies that have noted its importance for mesovortex development (e.g., Weisman and Trapp 2003). Additional analysis, particularly additional null cases (i.e., cases of rotating updrafts not resulting in TLV formation) is necessary to determine how common this is.

We acknowledge that the pathway described by Trapp et al. (2017) linking supercell updrafts and downdrafts to the development of near-ground rotation may not directly apply to QLCS tornadoes, as this pathway assumes the preexistence of an isolated, quasi-steady rotating updraft. For some of the TLVs examined herein, significant near-surface vertical vorticity precedes the development of a strong low-level updraft. Thus, in these cases, the initial development of rotation at the surface may not be directly dependent upon the characteristics of the tornadic updraft, but rather impacted by the characteristics of preceding and other nearby updrafts. For other tornadoes, the development of strong near-surface rotation follows the development of the updraft, as in supercells. Regardless of which path is followed, however, based upon Kelvin's circulation theorem, the circulation of the initial vortex should act as a constraint on initial intensity of the tornado.

Note again that the storm environment used herein is characteristic of a warm-season severe weather event; however, many tornadic QLCS events occur during the cool season (e.g., Thompson et al. 2012). While we expect that the findings discussed herein will be applicable to QLCSs in typical cool-season environments, it is unclear to what extent, such as those that pertain to parcel buoyancy and cold pool dynamics.

Future work will involve circuit analysis to understand how pretornadic near-surface vertical vorticity results in tornadoes to examine if and how the contraction of near-surface rotation occurs during tornado formation as described by the conceptual model proposed by Trapp et al. (2017). Additional analysis will be performed to determine the sources of tornadic and updraft vertical vorticity in QLCSs. Further, the processes leading to the development of bowing segments in QLCSs will be examined to identify possible precursors, as their existence appears to be associated with deep, rotating updraft development and tornado formation.

REFERENCES

Ashley, W. S., 2007: Spatial and temporal analysis of tornado fatalities in the United States: 1880–2005. *Wea. Forecasting*, **22**, 1214–1228, https://doi.org/10.1175/2007WAF2007004.1.

——, A. J. Krmenec, and R. Schwantes, 2008: Vulnerability due to nocturnal tornadoes. *Wea. Forecasting*, **23**, 795–807, https://doi.org/10.1175/2008WAF2222132.1.

——, A. M. Haberlie, and J. Strohm, 2019: A climatology of quasi-linear convective systems and their hazards in the United States. *Wea. Forecasting*, **34**, 1605–1631, https://doi.org/10.1175/WAF-D-19-0014.1.

Atkins, N. T., and M. St. Laurent, 2009a: Bow echo mesovortices. Part I: Processes that influence their damaging potential. *Mon. Wea. Rev.*, **137**, 1497–1513, https://doi.org/10.1175/2008MWR2649.1.

——, and ——, 2009b: Bow echo mesovortices. Part II: Their genesis. *Mon. Wea. Rev.*, **137**, 1514–1532, https://doi.org/10.1175/2008MWR2650.1.

——, J. M. Arnott, R. W. Przybylinski, R. A. Wolf, and B. D. Ketcham, 2004: Vortex structure and evolution within bow echoes. Part I: Single-Doppler and damage analysis of the 29 June 1998 derecho. *Mon. Wea. Rev.*, **132**, 2224–2242, https://doi.org/10.1175/1520-0493(2004)132<2224:VSAEWB>2.0.CO;2.

——, C. S. Bouchard, R. W. Przybylinski, R. J. Trapp, and G. Schmocker, 2005: Damaging surface wind mechanisms within the 10 June 2003 Saint Louis bow echo during BAMEX. *Mon. Wea. Rev.*, **133**, 2275–2296, https://doi.org/10.1175/MWR2973.1.

——, A. McGee, R. Ducharme, R. M. Wakimoto, and J. Wurman, 2012: The LaGrange tornado during VORTEX2. Part II: Photogrammetric analysis of the tornado combined with dual-Doppler radar data. *Mon. Wea. Rev.*, **140**, 2939–2958, https://doi.org/10.1175/MWR-D-11-00285.1.

Brooks, H. E., 2004: On the relationship of tornado path length and width to intensity. *Wea. Forecasting*, **19**, 310–319, https://doi.org/10.1175/1520-0434(2004)019<0310:OTROTP>2.0.CO;2.

Brotzge, J. A., S. E. Nelson, R. L. Thompson, and B. T. Smith, 2013: Tornado probability of detection and lead time as a function of

convective mode and environmental parameters. *Wea. Forecasting*, **28**, 1261–1276, https://doi.org/10.1175/WAF-D-12-00119.1.

Bryan, G. H., and J. M. Fritsch, 2002: A benchmark simulation for moist nonhydrostatic numerical models. *Mon. Wea. Rev.*, **130**, 2917–2928, https://doi.org/10.1175/1520-0493(2002)130<2917:ABSFMN>2.0.CO;2.

Carbone, R. E., 1982: A severe frontal rainband. Part I. Stormwide hydrodynamic structure. *J. Atmos. Sci.*, **39**, 258–279, https://doi.org/10.1175/1520-0469(1982)039<0258:ASFRPI>2.0.CO;2.

——, 1983: A severe frontal rainband. Part II: Tornado parent vortex circulation. *J. Atmos. Sci.*, **40**, 2639–2654, https://doi.org/10.1175/1520-0469(1983)040<2639:ASFRPI>2.0.CO;2.

Coffer, B. E., and M. D. Parker, 2017: Simulated supercells in nontornadic and tornadic VORTEX2 environments. *Mon. Wea. Rev.*, **145**, 149–180, https://doi.org/10.1175/MWR-D-16-0226.1.

Conrad, D. M., and K. R. Knupp, 2019: Doppler radar observations of horizontal shearing instability in quasi-linear convective systems. *Mon. Wea. Rev.*, **147**, 1297–1318, https://doi.org/10.1175/MWR-D-18-0257.1.

Deardorff, J. W., 1980: Stratocumulus-capped mixed layers derived from a three-dimensional model. *Bound.-Layer Meteor.*, **18**, 495–527, https://doi.org/10.1007/BF00119502.

Evans, J. S., and C. A. Doswell III, 2001: Examination of derecho environments using proximity soundings. *Wea. Forecasting*, **16**, 329–342, https://doi.org/10.1175/1520-0434(2001)016<0329:EODEUP>2.0.CO;2.

Fiedler, B. H., and R. Rotunno, 1986: A theory for the maximum windspeeds in tornado-like vortices. *J. Atmos. Sci.*, **43**, 2328–2340, https://doi.org/10.1175/1520-0469(1986)043<2328:ATOTMW>2.0.CO;2.

Flournoy, M. D., and M. C. Coniglio, 2019: Origins of vorticity in a simulated tornadic mesovortex observed during PECAN on 6 July 2015. *Mon. Wea. Rev.*, **147**, 107–134, https://doi.org/10.1175/MWR-D-18-0221.1.

——, ——, E. N. Rasmussen, J. C. Furtado, and B. E. Coffer, 2020: Modes of storm-scale variability and tornado potential in VORTEX2 near- and far-field tornadic environments. *Mon. Wea. Rev.*, **148**, 4185–4207, https://doi.org/10.1175/MWR-D-20-0147.1.

French, A. J., and M. D. Parker, 2012: Observations of mergers between squall lines and isolated supercell thunderstorms. *Wea. Forecasting*, **27**, 255–278, https://doi.org/10.1175/WAF-D-11-00058.1.

Funk, T. W., K. E. Darmofal, J. D. Kirkpatrick, V. L. Dewald, R. W. Przybylinski, G. K. Schmocker, and Y.-J. Lin, 1999: Storm reflectivity and mesocyclone evolution associated with the 15 April 1994 squall line over Kentucky and southern Indiana. *Wea. Forecasting*, **14**, 976–993, https://doi.org/10.1175/1520-0434(1999)014<0976:SRAMEA>2.0.CO;2.

Haurwitz, B., 1949: The instability of wind discontinuities and shear zones in planetary atmospheres. *J. Meteor.*, **6**, 200–206, https://doi.org/10.1175/1520-0469(1949)006<0200:TIOWDA>2.0.CO;2.

Houston, A. L., 2017: The possible role of density current dynamics in the generation of low-level vertical vorticity in supercells. *J. Atmos. Sci.*, **74**, 3191–3208, https://doi.org/10.1175/JAS-D-16-0227.1.

Kobayashi, F., Y. Sugawara, M. Imai, M. Matsui, A. Yoshida, and Y. Tamura, 2007: Tornado generation in a narrow cold frontal rainband—Fujisawa tornado on April 20, 2006. *SOLA*, **3**, 21–24, https://doi.org/10.2151/sola.2007-006.

Lebo, Z. J., and H. Morrison, 2015: Effects of horizontal and vertical grid spacing on mixing in simulated squall lines and

implications for convective strength and structure. *Mon. Wea. Rev.*, **143**, 4355–4375, https://doi.org/10.1175/MWR-D-15-0154.1.

Lee, B. D., and R. B. Wilhelmson, 1997a: The numerical simulation of non-supercell tornadogenesis. Part I: Initiation and evolution of pretornadic misocyclone circulations along a dry outflow boundary. *J. Atmos. Sci.*, **54**, 32–60, https://doi.org/10.1175/1520-0469(1997)054<0032:TNSONS>2.0.CO;2.

——, and ——, 1997b: The numerical simulation of non-supercell tornadogenesis. Part II: Evolution of a family of tornadoes along a weak outflow boundary. *J. Atmos. Sci.*, **54**, 2387–2415, https://doi.org/10.1175/1520-0469(1997)054<2387:TNSONT>2.0.CO;2.

Mansell, E. R., C. L. Ziegler, and E. C. Bruning, 2010: Simulated electrification of a small thunderstorm with two-moment bulk microphysics. *J. Atmos. Sci.*, **67**, 171–194, https://doi.org/10.1175/2009JAS2965.1.

Marion, G. R., and R. J. Trapp, 2019: The dynamical coupling of convective updrafts, downdrafts, and cold pools in simulated supercell thunderstorms. *J. Geophys. Res. Atmos.*, **124**, 664–683, https://doi.org/10.1029/2018JD029055.

——, ——, and S. W. Nesbitt, 2019: Using overshooting top area to discriminate potential for large, intense tornadoes. *Geophys. Res. Lett.*, **46**, 12 520–12 526, https://doi.org/10.1029/2019GL084099.

Markowski, P. M., 2018: A review of the various treatments of the surface momentum flux in severe storms simulations: Assumptions, deficiencies, and alternatives. *29th Conf. on Severe Local Storms*, Stowe, VT, Amer. Meteor. Soc., 7.3, https://ams.confex.com/ams/29SLS/webprogram/Paper348116.html.

——, and Y. Richardson, 2014: The influence of environmental low-level shear and cold pools on tornadogenesis: Insights from idealized simulations. *J. Atmos. Sci.*, **71**, 243–275, https://doi.org/10.1175/JAS-D-13-0159.1.

——, and G. H. Bryan, 2016: LES of laminar flow in the PBL: A potential problem for convective storm simulations. *Mon. Wea. Rev.*, **144**, 1841–1850, https://doi.org/10.1175/MWR-D-15-0439.1.

——, Y. Richardson, M. Majcen, J. Marquis, and J. Wurman, 2011: Characteristics of the wind field in three nontornadic low-level mesocyclones observed by the Doppler on Wheels radars. *Electron. J. Severe Storms Meteor.*, **6** (3), http://www.ejssm.org/ojs/index.php/ejssm/article/view/75/63.

Miles, J. W., and L. N. Howard, 1964: Note on a heterogeneous shear flow. *J. Fluid Mech.*, **20**, 331–336, https://doi.org/10.1017/S0022112064001252.

Mulder, K. J., and D. M. Schultz, 2015: Climatology, storm morphologies, and environments of tornadoes in the British Isles: 1980–2012. *Mon. Wea. Rev.*, **143**, 2224–2240, https://doi.org/10.1175/MWR-D-14-00299.1.

Orf, L., R. Wilhelmson, B. Lee, C. Finley, and A. Houston, 2017: Evolution of a long-track violent tornado within a simulated supercell. *Bull. Amer. Meteor. Soc.*, **98**, 45–68, https://doi.org/10.1175/BAMS-D-15-00073.1.

Przybylinski, R. W., 1995: The bow echo: Observations, numerical simulations, and severe weather detection methods. *Wea. Forecasting*, **10**, 203–218, https://doi.org/10.1175/1520-0434(1995)010<0203:TBEONS>2.0.CO;2.

——, G. K. Schmocker, and Y. J. Lin, 2000: A study of storm and vortex morphology during the 'intensifying stage' of severe wind mesoscale convective systems. Preprints, *20th Conf. on Severe Local Storms*, Orlando, FL, Amer. Meteor. Soc., 6.2, https://ams.confex.com/ams/Sept2000/webprogram/Paper16397.html.

Richter, H., J. Peter, and S. Collis, 2014: Analysis of a destructive wind storm on 16 November 2008 in Brisbane, Australia. *Mon. Wea. Rev.*, **142**, 3038–3060, https://doi.org/10.1175/MWR-D-13-00405.1.

Rotunno, R., 1985: On the rotation and propagation of simulated supercell thunderstorms. *J. Atmos. Sci.*, **42**, 271–292, https://doi.org/10.1175/1520-0469(1985)042<0271:OTRAPO>2.0.CO;2.

——, J. B. Klemp, and M. L. Weisman, 1988: A theory for strong, long-lived squall lines. *J. Atmos. Sci.*, **45**, 463–485, https://doi.org/10.1175/1520-0469(1988)045<0463:ATFSLL>2.0.CO;2.

Schaumann, J. S., and R. W. Przybylinski, 2012: Operational application of 0–3 km bulk shear vectors in assessing quasi linear convective system mesovortex and tornado potential. *26th Conf. on Severe Local Storms*, Nashville, TN, Amer. Meteor. Soc., 142, https://ams.confex.com/ams/26SLS/webprogram/Paper212008.html.

Schenkman, A. D., M. Xue, and A. Shapiro, 2012: Tornadogenesis in a simulated mesovortex within a mesoscale convective system. *J. Atmos. Sci.*, **69**, 3372–3390, https://doi.org/10.1175/JAS-D-12-038.1.

Sessa, M. F., and R. J. Trapp, 2020: Observed relationship between tornado intensity and pre-tornadic mesocyclone characteristics. *Wea. Forecasting*, **35**, 1243–1261, https://doi.org/10.1175/WAF-D-19-0099.1.

Smart, D. J., and K. A. Browning, 2009: Morphology and evolution of cold-frontal misocyclones. *Quart. J. Roy. Meteor. Soc.*, **135**, 381–393, https://doi.org/10.1002/qj.399.

Smith, B. T., R. L. Thompson, J. S. Grams, C. Broyles, and H. E. Brooks, 2012: Convective modes for significant severe thunderstorms in the contiguous United States. Part I: Storm classification and climatology. *Wea. Forecasting*, **27**, 1114–1135, https://doi.org/10.1175/WAF-D-11-00115.1.

Sugawara, Y., and F. Kobayashi, 2009: Vertical structure of misocyclones along a narrow cold frontal rainband. *J. Meteor. Soc. Japan*, **87**, 497–503, https://doi.org/10.2151/jmsj.87.497.

Thompson, R. L., B. T. Smith, J. S. Grams, A. R. Dean, and C. Broyles, 2012: Convective modes for significant severe thunderstorms in the contiguous United States. Part II: Supercell and QLCS tornado environments. *Wea. Forecasting*, **27**, 1136–1154, https://doi.org/10.1175/WAF-D-11-00116.1.

Trapp, R. J., 2000: A clarification of vortex breakdown and tornadogenesis. *Mon. Wea. Rev.*, **128**, 888–895, https://doi.org/10.1175/1520-0493(2000)128<0888:ACOVBA>2.0.CO;2.

——, and M. L. Weisman, 2003: Low-level mesovortices within squall lines and bow echoes. Part II: Their genesis and implications. *Mon. Wea. Rev.*, **131**, 2804–2823, https://doi.org/10.1175/1520-0493(2003)131<2804:LMWSLA>2.0.CO;2.

——, E. D. Mitchell, G. A. Tipton, D. W. Effertz, A. I. Watson, D. L. Andra Jr., and M. A. Magsig, 1999: Descending and nondescending tornadic vortex signatures detected by WSR-88Ds. *Wea. Forecasting*, **14**, 625–639, https://doi.org/10.1175/1520-0434(1999)014<0625:DANTVS>2.0.CO;2.

——, S. A. Tessendorf, E. S. Godfrey, and H. E. Brooks, 2005: Tornadoes from squall lines and bow echoes. Part I: Climatological distribution. *Wea. Forecasting*, **20**, 23–34, https://doi.org/10.1175/WAF-835.1.

——, G. R. Marion, and S. W. Nesbitt, 2017: The regulation of tornado intensity by updraft width. *J. Atmos. Sci.*, **74**, 4199–4211, https://doi.org/10.1175/JAS-D-16-0331.1.

——, ——, and ——, 2018: Reply to "Comments on 'The regulation of tornado intensity by updraft width.'" *J. Atmos. Sci.*, **75**, 4057–4061, https://doi.org/10.1175/JAS-D-18-0276.1.

Weisman, M. L., and R. J. Trapp, 2003: Low-level mesovortices within squall lines and bow echoes. Part I: Overview and dependence on environmental shear. *Mon. Wea. Rev.*, **131**, 2779–2803, https://doi.org/10.1175/1520-0493(2003)131<2779:LMWSLA>2.0.CO;2.

Wheatley, D. M., and R. J. Trapp, 2008: The effect of mesoscale heterogeneity on the genesis and structure of mesovortices within quasi-linear convective systems. *Mon. Wea. Rev.*, **136**, 4220–4241, https://doi.org/10.1175/2008MWR2294.1.

——, ——, and N. T. Atkins, 2006: Radar and damage analysis of severe bow echoes observed during BAMEX. *Mon. Wea. Rev.*, **134**, 791–806, https://doi.org/10.1175/MWR3100.1.

Wicker, L. J., and R. B. Wilhelmson, 1995: Simulation and analysis of tornado development and decay within a three-dimensional supercell thunderstorm. *J. Atmos. Sci.*, **52**, 2675–2703, https://doi.org/10.1175/1520-0469(1995)052<2675:SAAOTD>2.0.CO;2.